ACS APPLIED MATERIALS & INTERFACES

Research Article

Cite This: ACS Appl. Mater. Interfaces 2019, 11, 1821−1828

www.acsami.org

Three-Dimensional CeO_2 Woodpile Nanostructures To Enhance Performance of Enzymatic Glucose Biosensors

Yiliang Zhou, Sema Demirci Uzun, Nicholas J. Watkins, Shengkai Li, Wenhao Li, Alejandro L. Briseno, Kenneth R. Carter,* and James J. Watkins*

Department of Polymer Science and Engineering, University of Massachusetts Amherst, Amherst, Massachusetts 01003, United States

Supporting Information

ABSTRACT: Fabrication of detection elements with ultrahigh surface area is essential for improving the sensitivity of analyte detection. Here, we report a direct patterning technique to fabricate three-dimensional CeO_2 nanoelectrode arrays for biosensor application over relatively large areas. The fabrication approach, which employs nanoimprint lithography and a CeO_2 nanoparticle-based ink, enables the direct, high-throughput patterning of nanostructures and is scalable, integrable, and of low cost. With the convenience of sequential imprinting, multilayered woodpile nanostructures with prescribed numbers of layers were achieved in a "stacked-up" architecture and were successfully fabricated over large areas. To demonstrate application as a biosensor, an enzymatic glucose sensor was developed. The sensitivity of glucose sensors can be enhanced simply by increasing the number of layers, which multiplies surface area while maintaining a constant footprint. The four-layer woodpile nanostructure of CeO_2 glucose sensor exhibited enhanced sensitivity (42.8 μA mM^{-1} cm^{-2}) and good selectivity. This direct imprinting strategy for three-dimensional sensing architectures is potentially extendable to other electroactive materials and other sensing applications.

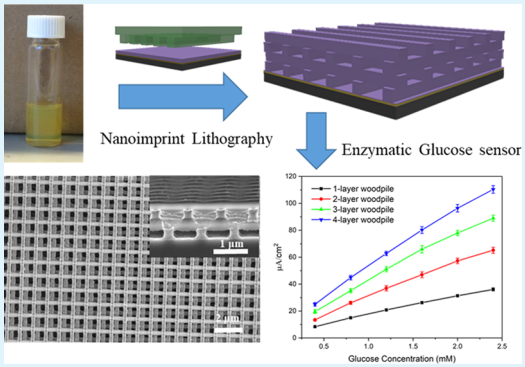

KEYWORDS: *nanoimprint lithography, direct patterning techniques, 3D nanostructures, glucose sensor, biosensor*

1. INTRODUCTION

High-sensitivity biosensors are widely sought for applications including clinical chemistry, on-body health monitoring, biological analyses, as well as safety and quality assurance in the food industry.[1−3] Among a multitude of sensing materials, nanostructured metal oxides have received significant attention due to their large surface-to-volume ratio and excellent selectivity when coupled to biorecognition molecules.[4,5] Various kinds of metal oxide nanomaterials, such as nanorods, nanowires, nanofibers, nanocombs, nanotubes, have been synthesized for sensor applications.[6−9] Of these, only a few reports focused on utilizing advanced processing techniques for developing these nanomaterials into even more efficient sensing components. To date, direct printing techniques, such as inkjet printing and direct laser writing, have emerged as favorable fabrication methods for producing micro-/nanostructured materials as sensing elements.[10−14] For example, Adly et al. developed inkjet-printed flexible microgap electrodes for ssDNA detection.[15] Although these direct printing techniques are potentially scalable and designable, the main challenge for applications in producing nanostructured materials is to maintain both high resolution and high manufacturing rate and scalability.

Nanoimprint lithography (NIL) offers a promising low-cost, high-throughput, direct patterning method to fabricate two-dimensional and three-dimensional (3D) nanostructures.[16−19] A wide variety of materials have been applied for patterning, including self-assembled monolayers,[20] polymers[21,22] and inorganic sol−gel materials.[23] More recently, inorganic nanoparticles and nanotubes were directly patterned into various architectures. For example, Au nanoparticles stabilized with bulky ionic liquid ligands resulting in a composition of 53 wt % Au (<10 vol % Au) and indium tin oxide (ITO) nanoparticle solution were directly utilized for surface patterning via NIL.[24,25] Nevertheless, the aspect ratios of previously reported inorganic imprinted structures, made by NIL, were generally limited. This is due to the low stamp modulus,[26] insufficient mass transfer,[27] and the volumetric shrinkage with ink drying.[28] In the case of ITO imprinting done at very high temperatures led to poor feature replication, oxygen vacancies in the ITO, low transparency, and aspect ratios much smaller than 1. Limited aspect ratio is detrimental to the total surface area of the nanostructures and limits their sensing performance. To solve this problem, a general imprinting approach was developed for fabricating 3D crystalline metal oxide nanostructures, including woodpile nanostructures.[29−31] Ink comprised predominantly of crystalline nanoparticles was directly patterned into nanostructures via NIL. The woodpile

Received: September 28, 2018
Accepted: December 24, 2018
Published: December 24, 2018

DOI: 10.1021/acsami.8b16985
ACS Appl. Mater. Interfaces 2019, 11, 1821−1828

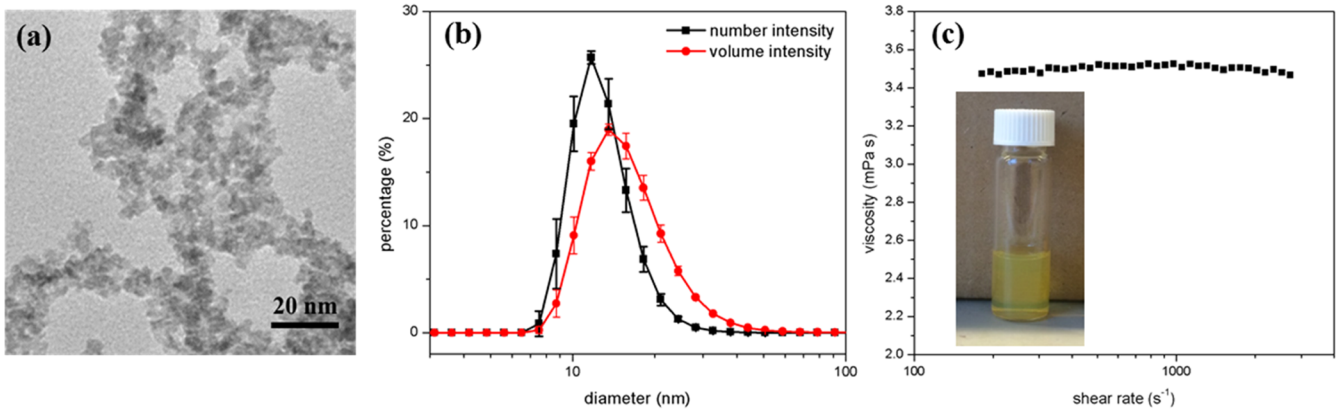

Figure 1. (a) TEM image of CeO_2 nanoparticles. (b) Particle size distribution of ceria in methanol by DLS. (c) Shear viscosity of the CeO_2 ink under shear rate between 200 and 2000 s^{-1} (inset image shows well-dispersed CeO_2 nanoparticle dispersion).

nanostructures were obtained via sequential imprint-planarization cycles. Finally, the polymer planarization layers were removed via heating. The number of layers can be easily controlled by the number of imprint-planarization cycles. This simple stacking method enables the engineering of 3D nanoarchitectures with high and user-customized aspect ratios.

Here, we introduce a scalable approach for fabricating multilayer CeO_2 woodpile nanostructures for enzymatic glucose sensors using solvent-assisted NIL. Multiple layers of CeO_2 nanogratings can be sequentially stacked on each other, forming a high-aspect-ratio structure. As the number of imprinted layers increases, the sensitivity of the CeO_2 woodpile structure for glucose sensing exhibited a proportional enhancement due to the accompanying increase in total surface area. This result further demonstrated that woodpile nanostructures, as well-organized 3D immobilization matrices, are highly compatible with the enzyme-based detection schemes. The limitations on sensitivity supported by the weak electron transfer between the redox centers of enzyme and the immobilization matrix are reduced by tuning molecular architecture on the electrode surface. The controlled increase in the surface area of woodpile nanostructures serves to be of efficient use of the materials, yielding both good sensitivity and stability. Furthermore, NIL is widely compatible with micro/nanofabrication process, yielding a scalable platform technology for the integration of biosensing elements into microdevices.

2. EXPERIMENTAL SECTION

2.1. Fabrication of Poly(dimethylsiloxane) (PDMS) Mold. PDMS stamps were fabricated by casting PDMS into master molds. The PDMS precursor mixture contains 10:1 weight ratio of Sylgard 184 silicone elastomer base and curing agent. This mixture was degassed under vacuum for 20 min at room temperature. After thermal curing at 70 °C for 5 h, the PDMS stamps were removed from the molds.

2.2. Preparation of Ceria Nanoparticle Ink. A commercial colloidal dispersion of ceria nanoparticles, stabilized by acetate (Nyacol Nanotechnologies), referred to as CEO2(AC), was used as the ceria precursor. This ceria particle dispersion in water (20 wt %) was mixed with methanol and 1,2-propanediol in 1:2:2 weight ratio. This dispersion was further vortex-mixed and sonicated to obtain a ∼4 wt % ceria particle dispersion. Particle size and size distribution of ceria were characterized with transmission electron microscopy (TEM) (JEOL 2000FX) and Malvern Nano Zetasizer.

2.3. Preparation of Ceria Nanoparticle/Titania Sol−Gel Ink. Titanium diisopropoxide bis(acetylacetonate) (75 wt % in isopropanol, Sigma-Aldrich Co. Ltd.) was diluted with methanol to 10 wt %. Then, the titania sol was mixed with previous ∼4 wt % ceria particle dispersion as various volume ratios, such as 20:1 and 40:1, forming modified ceria ink.

2.4. Fabrication of Patterned and Multilayered Structure. The silicon wafer substrates were cleaned by sonication in ethanol and acetone for 5 min, followed by a piranha solution immersion for 2 h (3:1 volume ratio of sulfuric acid and hydrogen peroxide (30%)). The cleaned wafers were then rinsed with deionized water and dried. The nanoparticle-based ink was spin-coated on these wafer substrates at 3000 rpm for 150 s in a glovebox maintained at 5% relative humidity. The PDMS stamp was placed on the wet film at 55 °C for 10 min. The PDMS stamp was then removed, yielding patterned ceria film. The patterned film was calcined at 500 °C for 30 min to sinter the nanoparticles.

To obtain multilayered structures, a UV-cross-linkable low-viscosity organic thioleneacrylate prepolymer (NOA 60, Norland Products Inc.) was utilized as a sacrificial planarization layer. The calcined patterned film was first pretreated with low power oxygen plasma to lower the surface energy and improve the quality of the planarization layer. Then, a 10 wt % NOA 60 solution in propylene glycol monomethyl ether acetate solvent was spin-coated on the patterned film twice at 1000 rpm for 30 s with UV curing after each spin-coating step. The imprinting and planarization steps were then repeated. Finally, the CeO_2 structure was calcined at 500 °C for 2 h. As shown in Figure S1, the all-organic planarization layers can be completely removed with calcination.

As for the glucose sensor, patterned and multilayered CeO_2 woodpiles were fabricated on an Au/Ti (50/5 nm) bilayer-coated silicon wafer, deposited using an electron beam evaporator.

2.5. Immobilization of the GOx Enzyme. CeO_2 multilayered film was immersed into a solution of GOx (1 mg mL^{-1}) prepared in a 50 mM phosphate-buffered saline (PBS) solution mixed with Nafion (5%) overnight, allowing GOx immobilization to take place.[6] The electrode was then rinsed with PBS to wash away the nonimmobilized GOx and stored in 4 °C refrigerator for further use.

2.6. Preparation of the Glucose Solution. A glucose stock solution (0.1 M) was prepared with 50 mM PBS solution (pH 7.0). To ensure the formation of β-D-glucose, this stock solution was left at room temperature for 24 h before use.

2.7. Electrochemical Measurements. All electrochemical measurements were conducted using CHI 600D. The characterization of ceria electrodes was carried out with a three-electrode setup. A platinum wire served as the counter electrode, and the Ag/AgCl electrode worked as the reference electrode. The spectra of cyclic voltammetry (CV) curves were recorded in PBS (50 mM, pH 7.0) containing a 5 mM $Fe(CN)_6^{3-}$ solution. For amperometric studies, all experiments were carried out in PBS (50 mM, pH 7.0) via application of +0.7 V versus Ag/AgCl electrode. The glucose sensing was conducted under mild stirring at room temperature. After each

DOI: 10.1021/acsami.8b16985
ACS Appl. Mater. Interfaces 2019, 11, 1821−1828

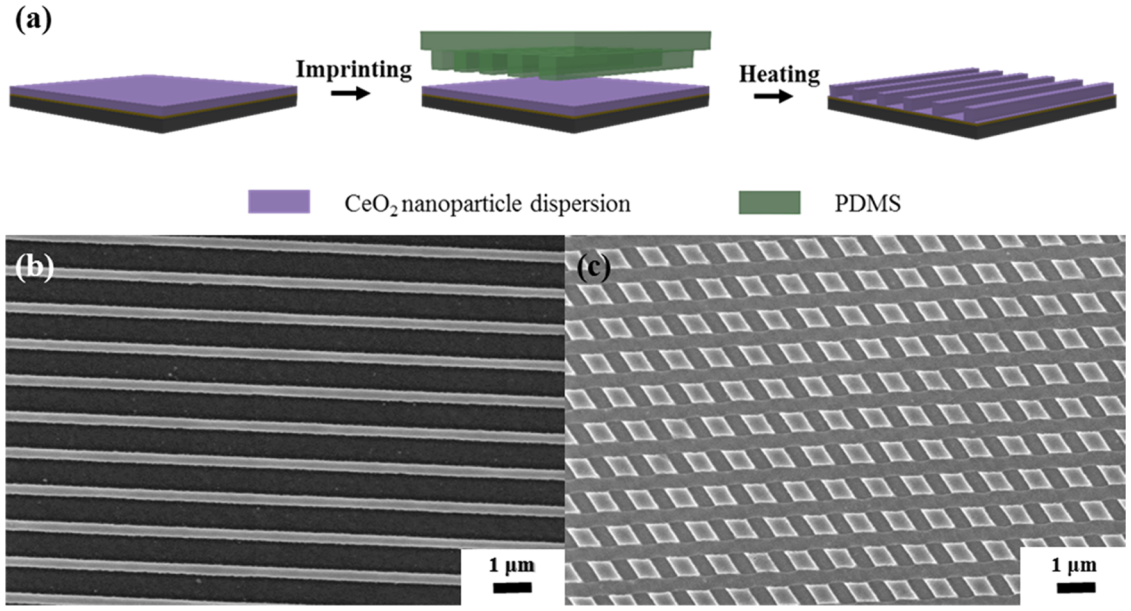

Figure 2. (a) Illustration of fabrication steps for obtaining patterned CeO_2 film via solvent-assisted nanoimprint lithography with ceria nanoparticles; (b, c) SEM images of patterned CeO_2 films with different structures (grating line and nanopillar structures with 500 nm width).

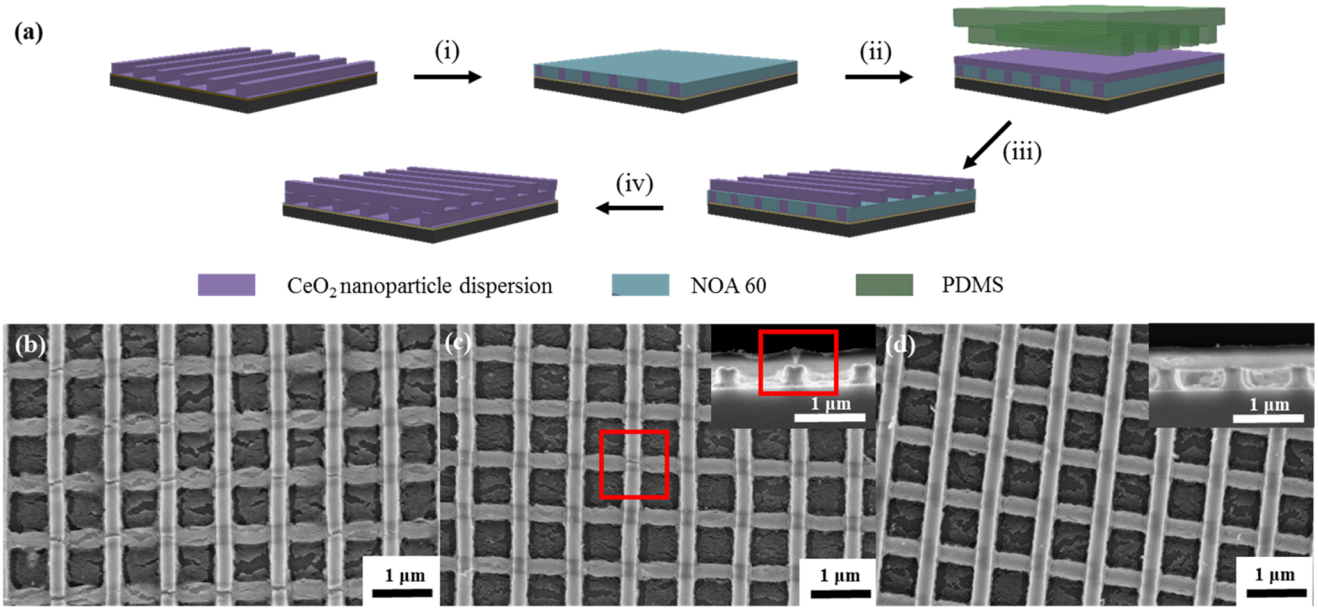

Figure 3. (a) Schematic illustration of steps to fabricate bilayer structure of CeO_2 film via solution-based soft nanoimprint lithography. (i) Planarization with a thiol−ene-based photopolymer. (ii) Spin coating new layer. (iii) Second-layer imprinting with molding−drying−demolding process. (iv) Two-layer woodpile electrode obtained after calcination; (b−d) SEM images of bilayer nanostructures with (b) pure CeO_2 nanoparticles, (c) CeO_2 nanoparticle with 2.5 vol % titanium sol gel and (d) CeO_2 nanoparticle with 5 vol % titanium sol gel.

measurement, the reaction cell and electrodes were fully washed with PBS (50 mM, pH 7.0) solution. Standard deviations of these measurements were calculated based on the average of three consecutive results.

3. RESULTS AND DISCUSSION

The first step for fabricating woodpile structure is to generate a stable imprintable CeO_2 ink. For solvent-assisted nanoimprint, ink's imprintability is mainly related with nanoparticle size, dispersity, solid concentration, and ink viscosity. Our imprint ink is made with commercial colloidal CeO_2 nanoparticle dispersions (20 wt %) in water (Nyacol Nanotechnologies). As shown in transmission electron microscopy (TEM) image, the ceria particle core size is below 10 nm (Figure 1a). The number- and volume-averaged particle sizes from dynamic light scattering (DLS) are 11.8 and 13.6 nm, respectively (Figure 1b). The difference is due to the solvation of the ligands. This ceria particle dispersion in water was mixed with methanol and 1,2-propanediol in 1:2:2 weight ratio to obtain a 4 wt % ceria nanoparticle dispersion, as the imprint ink. The incorporation of methanol and 1,2-propanediol is critical in two ways: (1) the low boiling point of methanol (bp 64.7 °C) leads to fast evaporation and quick concentration of the ink during spin-coating process, whereas the high boiling point solvent, 1,2-propanediol (bp 188.2 °C), ensures fluidity during the imprinting step; (2) the combination of these two solvents

DOI: 10.1021/acsami.8b16985
ACS Appl. Mater. Interfaces 2019, 11, 1821−1828

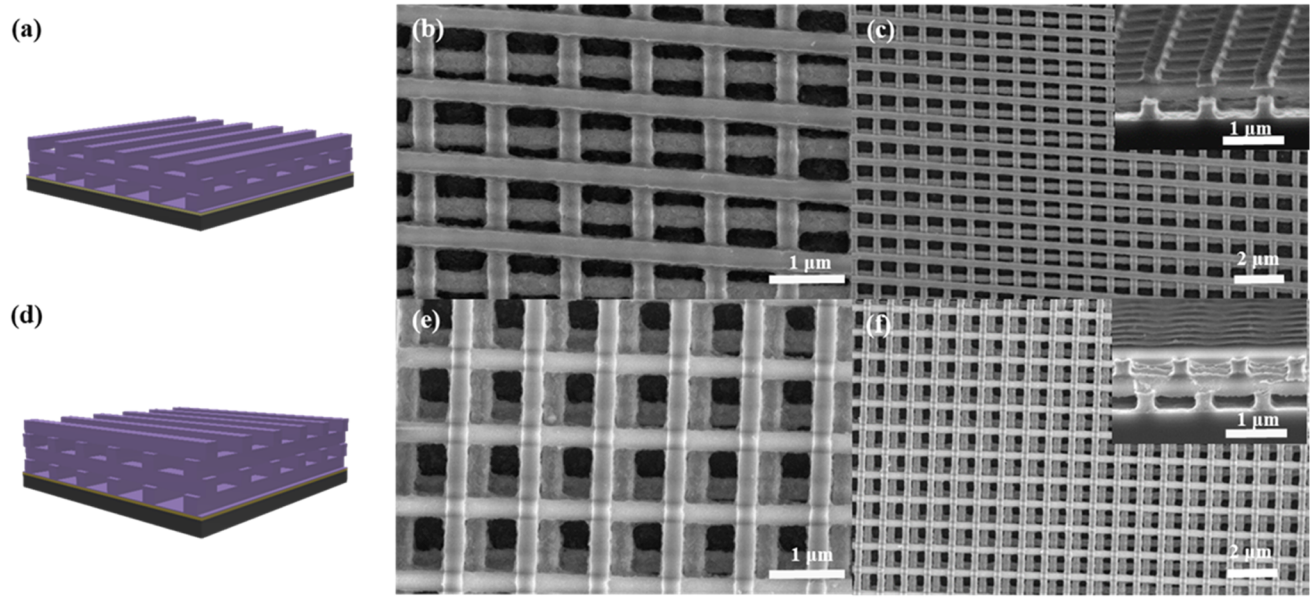

Figure 4. Schematic illustration of (a) three-layer and (d) four-layer CeO_2 woodpile nanostructures. SEM images of (b, c) trilayer and (e, f) tetralayer CeO_2 films with different magnifications. The insert images show cross-section SEM images of three- and four-layer CeO_2 woodpile nanostructures.

provides proper stability, viscosity, and wettability of ink for spin-coating processes.[29] The viscosity of ink remains low (3.5 mPa s), which is approximate to that of the mixture solvent (2.6 mPa s at 25 °C) (Figure 1c). Meanwhile, this CeO_2 ink is stable with negligible precipitation for several months. These properties of ink are important to mold filling and solvent-assisted nanoimprinting.

The schematic illustration of the process of solvent-assisted soft nanoimprint lithography with CeO_2 nanoparticles is shown in Figure 2a. A poly(dimethyl siloxane) (PDMS) stamp with lithographically designed structures was placed on the top of the spin-coated film. During heating, solvent was absorbed into the PDMS stamp, and a patterned film was obtained after demolding. Due to the effective dispersion and the small diameters of the nanoparticles in the ink (Figure 1), these ceria nanoparticles can be easily and rapidly imprinted to yield nanostructures over large areas. As shown in Figure 2b,c, CeO_2 nanostructures with various patterns were developed. The final architecture is obtained through a calcination process in air at 500 °C for 30 min. This high-temperature calcination completely removes the planarization layers and other organics. Thermal gravimetric analysis (TGA) curves of planarization layer and nanoparticle ink are shown in Figure S1. The difference in dimensions between the master mold and the printed CeO_2 film before and after annealing at 500 °C is discussed in detail in Figure S2.

To fabricate multilayered woodpile nanostructures, the planarization step is essential to enable imprinting of the succeeding layers. A commercial UV cross-linkable thiol−ene-based photopolymer (NOA 60, Norland Products Inc.) is applied as the planarization material. Photopolymer dispersion fills the trenches and forms a solid and planar surface with UV curing. The second layer of ceria nanoparticles was imprinted on this new planarization layer in an orthogonal orientation. Finally, the organic planarization layer is removed during calcination to build the two-layer woodpile nanostructure. The schematic illustration for these processes is shown in Figure 3a. However, cracks were observed when using pure CeO_2 nanoparticle ink, as shown in Figure 3b. All these defects happened at the intersections of two layers, caused by weak connectivity of the ceria particles following calcination. Though the neck formation and ripening of particles during calcination can enhance the mechanical properties of the nanostructure, the second layer of CeO_2 grating lines was still not strong enough to firmly stack on the first layer. To solve this, a binder for connecting nanoparticles together is needed for preventing cracks for multilayer stack. Here, a 10 wt % UV-curable binder, titanium diisopropoxide bis(acetylacetonate), in methanol/isopropanol was added to improve the mechanical strength of grating lines. Figure 3c,d shows the SEM images of bilayer woodpile nanostructures with addition of different amounts of titanium sol gel. When 2.5 vol % titanium sol gel was added into CeO_2 nanoparticle ink, a majority of the defects were eliminated; however, a few defects were still observed, which is marked in the red box (Figure 3c). Defects in the bilayer were essentially eliminated by adding 5 vol % titanium sol gel. SEM images show robust bilayers without any defects (Figure 3d). A defect-free imprint image with a larger area view (Figure S3) demonstrates the robustness of this method. X-ray photoelectron spectroscopy (XPS) indicates that the ratio of Ti/(Ti + Ce) is 4.93% in the material after calcination (Figure S4). The mass loss of this modified ink is slightly increased due to the addition of binder, as shown in Figure S1. X-ray diffraction (XRD) shows annealed sample with typical peaks corresponding to (111), (200), (220), (311) plane, which represents the face-centered cubic fluorite structure of CeO_2. The average crystallite size is calculated to be 6.1 nm. To be noticed, there is no additional peak from crystalline TiO_2 observed (Figure S5). This might due to the limited amount of binder and annealing condition.

With this modified CeO_2 ink, additional layers can be easily built upon the existing woodpile structure by simply repeating the fabrication steps. The SEM images of woodpiles with three and four layers are shown in Figure 4. The cross-sectional SEM images show that these grating lines were stacked firmly on the bottom layers. Well-defined nanogratings with aspect ratio of 1

DOI: 10.1021/acsami.8b16985
ACS Appl. Mater. Interfaces 2019, 11, 1821−1828

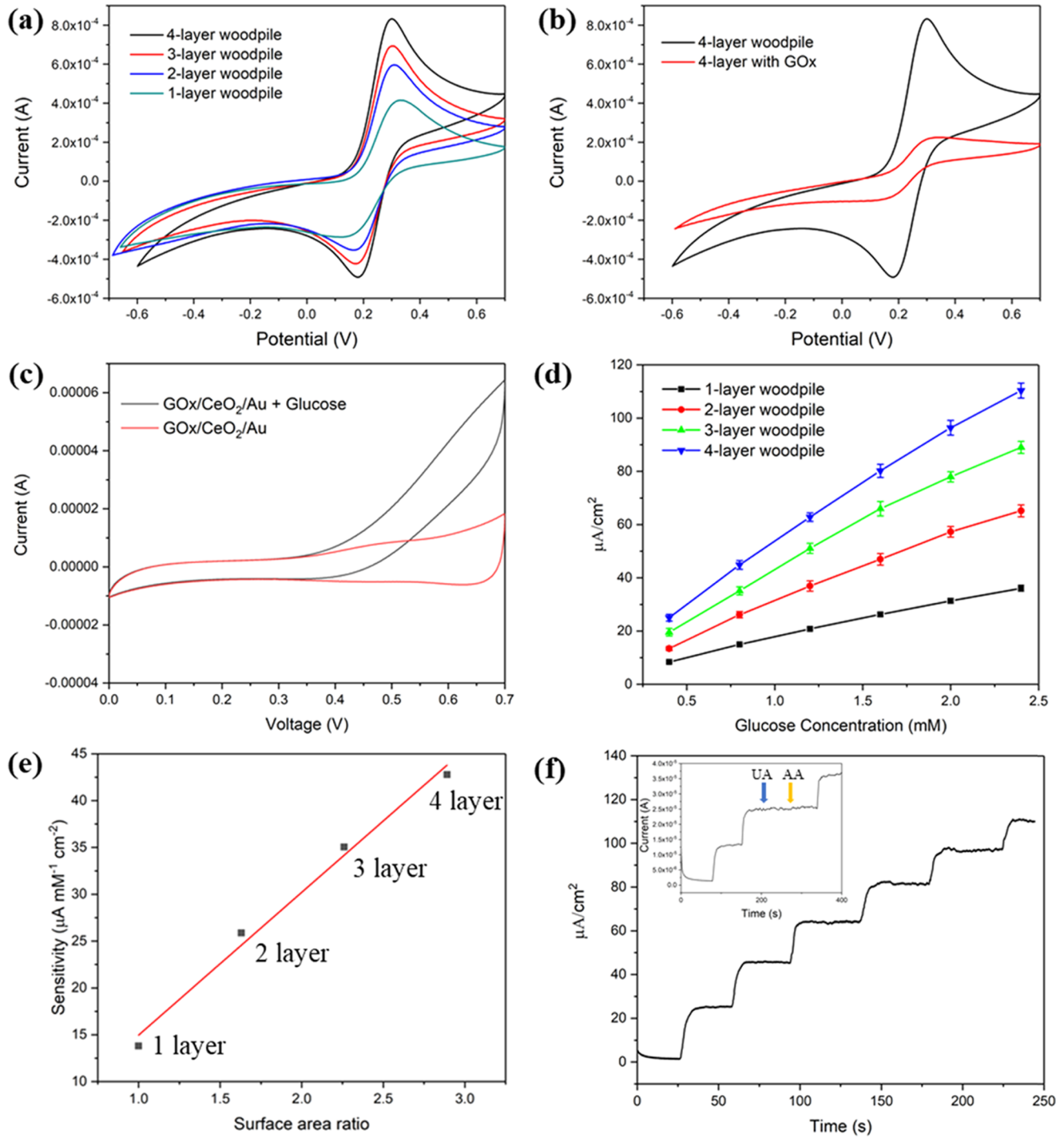

Figure 5. (a) Cyclic voltammograms of different layers of CeO_2 electrodes recorded in PBS (50 mM, pH 7.0) containing a 5 mM $Fe(CN)_6^{3-}$ solution. (b) Cyclic voltammograms of four-layer CeO_2 woodpile electrodes before and after modification with GOx. (c) Cyclic voltammograms of GOx/CeO_2/Au electrode with and without glucose. (d) Calibration curves for glucose with various layers of CeO_2 woodpile structure (with range of 0.4−2.4 mM). (e) The relationship between sensitivity and total surface area ratio with various layers of woodpile structure (all of the values of surface area ratio are based on the surface area of one-layer imprinting). (f) Amperometric response curve of the fabricated four-layer CeO_2 sensor with successive glucose injection. Each addition is 0.4 mM glucose. Inset image shows selectivity of sensors. 0.2 mM glucose, 0.2 mM ascorbic acid, and 0.2 mM uric acid were added. All measurements for glucose are conducted in PBS buffer solution (50 mM, pH 7.0, 25 °C, +0.7 V). Error bars in figures show the standard deviation of three measurements.

were obtained. The width and height are each approximately 230 nm. The dimensions are consistent in every layer. Consequently, stacking more layers results in higher aspect ratio. Notably, the dimensions of each layers and number of layers can be easily tuned using the desired master mold and number of imprint cycles. Meanwhile, as the number of layers increases, this woodpile nanostructure exhibits corresponding increases in surface area and more importantly a nearly constant surface-to-volume ratio, as the overlapping area between layers is negligible.

DOI: 10.1021/acsami.8b16985
ACS Appl. Mater. Interfaces 2019, 11, 1821−1828

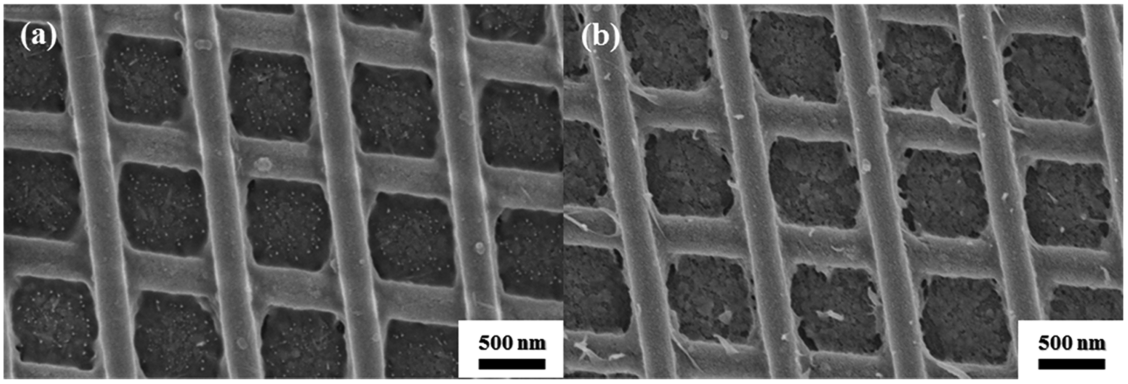

Figure 6. SEM images of woodpile electrodes with (a) GOx and (b) GOx and Nafion.

We then apply woodpile structures as a transducer for biosensor applications. Nanostructured CeO_2 exhibits many desirable properties, such as electrical conductivity, chemical inertness, nontoxicity, and biocompatibility.[32] To date, CeO_2 nanomaterials have been applied for detection of glucose,[32] cholesterol,[33] H_2O_2,[34] and DNA.[35] To demonstrate the benefits of this woodpile CeO_2 nanostructure in biosensor applications, we tested it as an enzymatic glucose sensor. Glucose has a notable importance in terms of both clinical studies to prevent and control diabetes as well as the food industry. The impact of the former is potentially significant as an estimated 422 million people, as reported by WHO in 2014, suffer from diabetes.[36]

Here, CeO_2 woodpile nanostructures with different numbers of layers were fabricated on a bilayer of Ti/Au (5/50 nm), which served as the current collector. First, cyclic voltammetry (CV) studies were conducted in PBS buffer (50 mM, pH 7.0) containing 5 mM $Fe(CN)_6^{3-}$ over the range of −0.7 to +0.7 V. Figure 5a shows that the peak current of ferrocyanide/ferricyanide increased with the number of layers, confirming that the woodpile nanostructures with more layers provide a higher surface area for faradaic electron transfer. The CV curves at various scan rates are shown in Figure S6. The linear relation between peak currents and the square root of the scan rates indicates that mass transfer between electrodes was a diffusion-controlled process, similar to other reported for surface-confined redox species on electrodes.[18]

Glucose oxidase (GOx) was immobilized on the CeO_2 via electrostatic interactions. CeO_2 is known as a material with high isoelectric point (IEP, 9.2). The high IEP indicates that CeO_2 carries positively electrical charge in a pH 7.0 buffer solution. This property renders CeO_2 particularly attractive for immobilization of low IEP enzymes (for example, glucose oxidase, GOx, exhibits an IEP of 4.2) via electrostatic interactions.[37] The addition of Nafion was applied to form a uniform film on the GOx/CeO_2 for improving the stability of immobilization.[38] Immobilization of GOx was confirmed using electrochemical characterization. The CV curve in Figure 5b shows that the peak current decreased after modification with GOx. This decreased peak current is a consequence of the insulating characteristics of GOx. SEM images of woodpile nanostructure after enzyme modification are shown in Figure 6. After immobilization, three-dimensional multilayer woodpile structure remains structurally stable. The nanostructure in two-layer woodpile electrode presents an increase in roughness, further indicating the successful immobilization of GOx on the woodpile surface. As shown in Figure 6b, a thin layer of Nafion film is coated on the woodpile electrode for optimizing the immobilization stability.

The cyclic voltammetry of the GOx/CeO_2/Au in a 50 mM PBS (pH 7.0) between 0 and +0.7 V against Ag/AgCl at a potential scan rate of 0.01 V s^{-1} is shown in Figure 5c. After adding 1 mM glucose into the solution, an obvious current increase can be observed above the +0.40 V potential, showing glucose is detectable at high potentials. Saha et al. proposed a mechanism for CeO_2-based glucose sensing, relying on the reoxidation of CeO_2.[37] Here, the performance of CeO_2 glucose sensor was tested using an amperometric technique in phosphate-buffered saline solution (PBS, 50 mM, pH 7.0, 25 °C) at an applied potential of +0.7 V. Before detailed measurements of sensor performance with various layers could be obtained, the effect of the addition of titanium sol gel needed to be studied. Thus, devices containing one layer of imprinted CeO_2 both with and without titanium sol gel were developed and examined. As shown in Figure S7, both samples exhibit similar sensitivity as a glucose sensor, indicating that the addition of titanium sol gel did not impact the performance. Moreover, these imprinted CeO_2 electrodes show good reproducibility and repeatability for glucose sensing (Figure S8).

Calibration curves for glucose (with range of 0.4−2.4 mM in PBS solution) with various layers of CeO_2 woodpile nanostructure were then generated and are shown in Figure 5d. The sensitivity of CeO_2 woodpile nanostructures increased systematically with the number of layers. The sensitivity with different numbers of layers exhibits a linear relationship with surface area of nanostructure (Figure 5e). The calculation of surface area is based on the dimension of the patterned line from SEM (230 nm width and 1000 nm pitch). The surface area includes the area of residue layer, and overlapping area between layers is negligible. This linear relationship reveals that the woodpile architecture not only provides high surface areas but also accessible area for biomaterials due to its hierarchical nanostructure. The sensitivity of four-layer woodpile of CeO_2 is 42.8 μA mM^{-1} cm^{-2}, a value that is approximately 3.1 times that of the sensitivity of single-layer devices (13.8 μA mM^{-1} cm^{-2}). The limit of detection was 10 μM at a signal to noise ratio of 3. Amperometric response of the four-layer woodpile of CeO_2/Au glucose biosensor on successive additions of 0.4 mM glucose with a response time of ∼5 s is shown in Figure 5f. A detailed real-time glucose detection is shown in Figure S9. Moreover, these woodpile sensors show good selectivity, as shown in Figure 5f. The electrode has a limited response to interferences, ascorbic acid,

DOI: 10.1021/acsami.8b16985
ACS Appl. Mater. Interfaces 2019, 11, 1821−1828

Table 1. Comparison of Glucose Sensor Performance of the Four-Layer CeO_2 Woodpile with Recent Reports on CeO_2

immobilization matrix	sensitivity (μA mM^{-1} cm^{-2})	limit of detection (μM)	K_m^{app}	linear range	applied potential (V)	refs
CeO_2 nanorods	0.165	100	44.57 mM	2−26 mM	+0.80	7
nanostructured CeO_2	0.517	12	13.55 μM	50−400 mg L^{-1}	+0.50	32
nanoporous CeO_2	NA	NA	1.01 mM	25−300 mg L^{-1}	+0.33	37
nano-CeO_2/graphene	7.198	2	3.5 mM	0.05−6.5 mM	+0.38	40
nanostructured CeO_2[a]	44	10	NA	1−10 mM	NA	41
CeO_2/polyaniline[a]	25.79	0.56	NA	NA	+0.10	42
CeO_2@CuO core shell[a]	3319.83	0.019	NA	1−8.9 μM	+0.40	43
four-layer CeO_2 woodpile	42.8	10	4.59 mM	0.02−2.5 mM	+0.70	this work

[a]Nonenzymatic glucose sensor.

and uric acid. This good selectivity is due to the incorporation of Nafion film. This perfluorinated cation-exchange polymer membrane can strongly restrict the passage of anions across the membrane.[39] The long-term stability of four-layer woodpile electrode is shown in Figure S10. The biosensor remains ∼88% of initial response after 3 weeks.

To demonstrate that the woodpile structure does in fact enhance sensor performance, a series of unpatterned CeO_2 electrodes were fabricated, and their performance was compared to the woodpile structures. For example, a CeO_2 film made by four spin-coating−calcination cycles is utilized as a control sample for the four-layer woodpile. As shown in Figure S11, although unpatterned CeO_2 exhibits similar sensing performance as patterned structure, performance difference becomes much larger as the number of layers increases. The sensitivity of four-layer woodpile structure is approximately 2.5 times that of the sensitivity of control sample with similar mass loading. This confirms that the woodpile stacking is effective for enhancing sensing performance.

Table 1 compares the sensitivity, limit of detection, value of the apparent Michaelis−Menten constant (K_m^{app}), and linear range with other CeO_2-based glucose sensors reported from literature.[7,32,37,40−43] These works mainly focus on CeO_2 with nanoscale morphologies (e.g., nanorod, nanoporous) or composite materials with CeO_2. Although we use commercially available particles, these relatively simple and scalable woodpile structures achieve comparable-to-better sensor performance among enzymatic glucose sensors with CeO_2-based nanomaterials. Moreover, even higher aspect ratio CeO_2 electrodes could be fabricated via the same strategy for achieving higher sensitivity. The mechanical strength and conductivity of the CeO_2 nanogratings determine their upper limit.

CONCLUSIONS

In summary, three-dimensional CeO_2 woodpile electrodes with designed aspect ratios were developed via solvent-assisted NIL for application as glucose biosensors. The biosensor results demonstrate that the sensitivity of this CeO_2 woodpile electrode can be increased by simply increasing the number of layers. The four-layer CeO_2 woodpile electrode has been proved as an excellent glucose sensor with enhanced performance. Moreover, this "stacked-up" approach with NIL enables one to redesign the dimensions of CeO_2 woodpile nanostructure (line width, line height, and number of layers) with different master molds for achieving various biosensor requirements. The method here is general and can be broadly applied to electroactive sensing materials.

ASSOCIATED CONTENT

Supporting Information

The Supporting Information is available free of charge on the ACS Publications website at DOI: 10.1021/acsami.8b16985.

TGA of NOA 60 and CeO_2 nanoparticles in air; SEM images of master mold and printed CeO_2 line before or after thermal anneal; SEM image of a larger area; XPS element scan of Ce and Ti; XRD of modified CeO_2 nanoparticle; CV of CeO_2 electrode at various scan rates; calibration curve of imprinted CeO_2 with and without binder; reproductivity and repeatability test of imprinted electrode; amperometric response curve of four-layer CeO_2 sensor to glucose injections; long-term stability of woodpile electrode; comparison of sensor performance in woodpiles and in planar films (PDF)

AUTHOR INFORMATION

Corresponding Authors

*E-mail: watkins@polysci.umass.edu (K.R.C.).
*E-mail: krcarter@polysci.umass.edu (J.J.W.).

ORCID

Yiliang Zhou: 0000-0003-3984-0763
Shengkai Li: 0000-0001-6825-4398
Wenhao Li: 0000-0003-2614-0768
Alejandro L. Briseno: 0000-0003-2981-9143
Kenneth R. Carter: 0000-0002-7081-2296

Notes

The authors declare no competing financial interest.

ACKNOWLEDGMENTS

This work was funded by the NSF Center for Hierarchical Manufacturing at the University of Massachusetts Amherst (CMMI-1025020). S.D.U. acknowledges to TÜBİTAK-BİDEB for Postdoctoral Scholarship.

REFERENCES

(1) Bahadır, E. B.; Sezginturk, M. K. Applications of Commercial Biosensors in Clinical, Food, Environmental, and Biothreat/Biowarfare Analyses. *Anal. Biochem.* **2015**, *478*, 107−120.

(2) Uzun, S. D.; Kayaci, F.; Uyar, T.; Timur, S.; Toppare, L. Bioactive Surface Design Based on Functional Composite Electrospun Nanofibers for Biomolecule Immobilization and Biosensor Applications. *ACS Appl. Mater. Interfaces* **2014**, *6*, 5235−5243.

(3) Uzun, S. D.; Unlu, N. A.; Sendur, M.; Kanik, F. E.; Timur, S.; Toppare, L. A Novel Promising Biomolecule Immobilization Matrix: Synthesis of Functional Benzimidazole Containing Conducting Polymer and Its Biosensor Applications. *Colloids Surf., B* **2013**, *112*, 74−80.

DOI: 10.1021/acsami.8b16985
ACS Appl. Mater. Interfaces 2019, 11, 1821−1828

(4) Rahman, M. M.; Ahammad, A. J.; Jin, J. H.; Ahn, S. J.; Lee, J. J. A Comprehensive Review of Glucose Biosensors Based on Nanostructured Metal-oxides. *Sensors* **2010**, *10*, 4855−4886.
(5) Hahn, Y.-B.; Ahmad, R.; Tripathy, N. Chemical and Biological Sensors Based on Metal Oxide Nanostructures. *Chem. Commun.* **2012**, *48*, 10369−10385.
(6) Pradhan, D.; Niroui, F.; Leung, K. T. High-performance, Flexible Enzymatic Glucose Biosensor Based on ZnO Nanowires Supported on a Gold-coated Polyester Substrate. *ACS Appl. Mater. Interfaces* **2010**, *2*, 2409−2412.
(7) Patil, D.; Dung, N. Q.; Jung, H.; Ahn, S. Y.; Jang, D. M.; Kim, D. Enzymatic Glucose Biosensor Based on CeO2 Nanorods Synthesized by Non-isothermal Precipitation. *Biosens. Bioelectron.* **2012**, *31*, 176−181.
(8) Ansari, A. A.; Alhoshan, M.; Alsalhi, M. S.; Aldwayyan, A. S. Nanostructured Metal Oxides Based Enzymatic Electrochemical Biosensors. In *Biosensors*; InTech, 2010; Chapter 2.
(9) Gomez, J. L.; Tigli, O. Zinc Oxide Nanostructures: from Growth to Application. *J. Mater. Sci.* **2013**, *48*, 612−624.
(10) Singh, M.; Haverinen, H. M.; Dhagat, P.; Jabbour, G. E. Inkjet Printing—Process and Its Applications. *Adv. Mater.* **2010**, *22*, 673−685.
(11) Luo, S.; Hoang, P. T.; Liu, T. Direct Laser Writing for Creating Porous Graphitic Structures and Their Use for Flexible and Highly Sensitive Sensor and Sensor Arrays. *Carbon* **2016**, *96*, 522−531.
(12) Yetisen, A.; Qasim, M.; Nosheen, S.; Wilkinson, T.; Lowe, C. Pulsed Laser Writing of Holographic Nanosensors. *J. Mater. Chem. C* **2014**, *2*, 3569−3576.
(13) Yeom, C.; Chen, K.; Kiriya, D.; Yu, Z.; Cho, G.; Javey, A. Large-Area Compliant Tactile Sensors Using Printed Carbon Nanotube Active-Matrix Backplanes. *Adv. Mater.* **2015**, *27*, 1561−1566.
(14) Hondred, J. A.; Breger, J. C.; Alves, N. J.; Trammell, S. A.; Walper, S. A.; Medintz, I. L.; Claussen, J. C. Printed Graphene Electrochemical Biosensors Fabricated by Inkjet Maskless Lithography for Rapid and Sensitive Detection of Organophosphates. *ACS Appl. Mater. Interfaces.* **2018**, *10*, 11125−11134.
(15) Adly, N.; Feng, L.; Krause, K. J.; Mayer, D.; Yakushenko, A.; Offenhäusser, A.; Wolfrum, B. Flexible Microgap Electrodes by Direct Inkjet Printing for Biosensing Application. *Adv. Biosyst.* **2017**, *1*, No. 1600016.
(16) Xia, Y. N.; Whitesides, G. M. Soft Lithography. *Angew. Chem., Int. Ed.* **1998**, *37*, 550−575.
(17) Hwang, J. K.; Cho, S.; Dang, J. M.; Kwak, E. B.; Song, K.; Moon, J.; Sung, M. M. Direct Nanoprinting by Liquid-bridge-mediated Nanotransfer Moulding. *Nat. Nanotechnol.* **2010**, *5*, 742−748.
(18) Chen, J.; Zhou, Y.; Wang, D.; He, F.; Rotello, V. M.; Carter, K. R.; Watkins, J. J.; Nugen, S. R. UV-nanoimprint Lithography as a Tool to Develop Flexible Microfluidic Devices for Electrochemical Detection. *Lab Chip* **2015**, *15*, 3086−3094.
(19) Zaumseil, J.; Meitl, M. A.; Hsu, J. W.; Acharya, B. R.; Baldwin, K. W.; Loo, Y.-L.; Rogers, J. A. Three-dimensional and Multilayer Nanostructures Formed by Nanotransfer Printing. *Nano Lett.* **2003**, *3*, 1223−1227.
(20) Love, J. C.; Estroff, L. A.; Kriebel, J. K.; Nuzzo, R. G.; Whitesides, G. M. Self-assembled Monolayers of Thiolates on Metals as a Form of Nanotechnology. *Chem. Rev.* **2005**, *105*, 1103−1170.
(21) Leitgeb, M.; Nees, D.; Ruttloff, S.; Palfinger, U.; Götz, J.; Liska, R.; Belegratis, M. R.; Stadlober, B. Multilength Scale Patterning of Functional Layers by Roll-to-roll Ultraviolet-light-assisted Nanoimprint Lithography. *ACS Nano* **2016**, *10*, 4926−4941.
(22) Park, J. Y.; Hendricks, N. R.; Carter, K. R. Solvent-assisted Soft Nanoimprint Lithography for Structured Bilayer Heterojunction Organic Solar Cells. *Langmuir* **2011**, *27*, 11251−11258.
(23) Li, M.; Tan, H.; Chen, L.; Wang, J.; Chou, S. Y. Large Area Direct Nanoimprinting of SiO 2−TiO 2 Gel Gratings for Optical Applications. *J. Vac. Sci. Technol., B: Nanotechnol. Microelectron.: Mater., Process., Meas., Phenom.* **2003**, *21*, 660−663.
(24) Yu, X.; Pham, J. T.; Subramani, C.; Creran, B.; Yeh, Y.-C.; Du, K.; Patra, D.; Miranda, O. R.; Crosby, A. J.; Rotello, V. M. Direct Patterning of Engineered Ionic Gold Nanoparticles via Nanoimprint Lithography. *Adv. Mater.* **2012**, *24*, 6330−6334.
(25) Lee, S. H.; Ha, N. Y. Nanostructured Indium-tin-oxide Films Fabricated by All-solution processing for Functional Transparent Electrodes. *Opt. Express* **2011**, *19*, 21803−21808.
(26) Huang, Y. Y.; Zhou, W.; Hsia, K. J.; Menard, E.; Park, J.-U.; Rogers, J. A.; Alleyne, A. G. Stamp Collapse in Soft Lithography. *Langmuir* **2005**, *21*, 8058−8068.
(27) Kim, E.; Xia, Y.; Whitesides, G. M. Micromolding in Capillaries: Applications in Materials Science. *J. Am. Chem. Soc.* **1996**, *118*, 5722−5731.
(28) Dinachali, S. S.; Saifullah, M. S. M.; Ganesan, R.; Thian, E. S.; He, C. A Universal Scheme for Patterning of Oxides via Thermal Nanoimprint Lithography. *Adv. Funct. Mater.* **2013**, *23*, 2201−2211.
(29) Li, W.; Zhou, Y.; Howell, I. R.; Gai, Y.; Naik, A. R.; Li, S.; Carter, K. R.; Watkins, J. J. Direct Imprinting of Scalable, High-Performance Woodpile Electrodes for Three-Dimensional Lithium-Ion Nanobatteries. *ACS Appl. Mater. Interfaces* **2018**, *10*, 5447−5454.
(30) Kothari, R.; Beaulieu, M. R.; Hendricks, N. R.; Li, S.; Watkins, J. J. Direct Patterning of Robust One-Dimensional, Two-Dimensional, and Three-Dimensional Crystalline Metal Oxide Nanostructures Using Imprint Lithography and Nanoparticle Dispersion Inks. *Chem. Mater.* **2017**, *29*, 3908−3918.
(31) Arisoy, F. D.; Kolewe, K. W.; Homyak, B.; Kurtz, I. S.; Schiffman, J. D.; Watkins, J. J. Bioinspired Photocatalytic Shark Skin Surfaces with Antibacterial and Antifouling Activity via Nanoimprint Lithography. *ACS Appl. Mater. Interfaces* **2018**, *10*, 20055.
(32) Ansari, A. A.; Solanki, P. R.; Malhotra, B. Sol-gel Derived Nanostructured Cerium Oxide Film for Glucose Sensor. *Appl. Phys. Lett.* **2008**, *92*, No. 263901.
(33) Zhang, M.; Yuan, R.; Chai, Y.; Wang, C.; Wu, X. Cerium Oxide−Graphene as the Matrix for Cholesterol Sensor. *Anal. Biochem.* **2013**, *436*, 69−74.
(34) Deng, L.; Chen, C.; Zhu, C.; Dong, S.; Lu, H. Multiplexed Bioactive Paper Based on GO@ SiO2@ CeO2 Nanosheets for a Low-cost Diagnostics Platform. *Biosens. Bioelectron.* **2014**, *52*, 324−329.
(35) Pautler, R.; Kelly, E. Y.; Huang, P.-J. J.; Cao, J.; Liu, B.; Liu, J. Attaching DNA to Nanoceria: Regulating Oxidase Activity and Fluorescence Quenching. *ACS Appl. Mater. Interfaces* **2013**, *5*, 6820−6825.
(36) Roglic, G. WHO Global Report on Diabetes: A Summary. *Int. J. Non-Commun. Dis.* **2016**, *1*, 3−8.
(37) Saha, S.; Arya, S. K.; Singh, S.; Sreenivas, K.; Malhotra, B.; Gupta, V. Nanoporous Cerium Oxide Thin Film for Glucose Biosensor. *Biosens. Bioelectron.* **2009**, *24*, 2040−2045.
(38) Xu, J.-J.; Yu, Z.-H.; Chen, H.-Y. Glucose Biosensors Prepared by Electropolymerization of P-chlorophenylamine with and without Nafion. *Anal. Chim. Acta* **2002**, *463*, 239−247.
(39) Yuan, C. J.; Hsu, C. L.; Wang, S. C.; Chang, K. S. Eliminating the Interference of Ascorbic Acid and Uric Acid to the Amperometric Glucose Biosensor by Cation Exchangers Membrane and Size Exclusion Membrane. *Electroanalysis* **2005**, *17*, 2239−2245.
(40) De, S.; Mohanty, S.; Nayak, S. K. Nano-CeO2 Decorated Graphene Based Chitosan Nanocomposites as Enzymatic Biosensing Platform: Fabrication and Cellular Biocompatibility Assessment. *Bioprocess Biosyst. Eng.* **2015**, *38*, 1671−1683.
(41) Gougis, M.; Tabet-Aoul, A.; Ma, D.; Mohamedi, M. Nanostructured Cerium Oxide Catalyst Support: Effects of Morphology on the Electroactivity of Gold toward Oxidative Sensing of Glucose. *Microchim. Acta* **2014**, *181*, 1207−1214.
(42) Zhang, J.; Guan, P.; Li, Y.; Li, W.; Guo, Q. Polyaniline/Cerium Oxide Hybrid Modified Carbon Paste Electrode for Non-enzymatic Glucose Detection. *Bull. Korean Chem. Soc.* **2016**, *37*, 985−986.
(43) Dayakar, T.; Rao, K. V.; Bikshalu, K.; Malapati, V.; Sadasivuni, K. K. Non-enzymatic Sensing of Glucose Using Screen-printed Electrode Modified with Novel Synthesized CeO2@ CuO Core Shell Nanostructure. *Biosens. Bioelectron.* **2018**, *111*, 166−173.

DOI: 10.1021/acsami.8b16985
ACS Appl. Mater. Interfaces 2019, 11, 1821−1828